RESEARCH REPORTS

AN EXPERIMENTAL STUDY OF VORTEX TUBES

HEISHICHIRÔ TAKAHAMA and KIN-ICHI KAWASHIMA

Department of Mechanical Engineering

(Received October 27, 1960)

I. Introduction

High velocity vortex flow in a vortex tube shows that high energy gas particles gather in the outer annular region and low energy gas particles in the inner back flow region according to their energy levels; by separating these particles skilfully we get hot gas and cold one simultaneously.

Many studies on the vortex tube have been made during last ten years or so, among which few experimental studies treated energy separation. The work by Hartnett and Eckert[1] is worth noticing among experimental studies treating flow phenomena in the vortex tube; they measured and discussed, under a definite condition, velocity profiles and energy or temprature profiles; additional studies on this theme under several different conditions have seemed to be necessary.

By the way, Pengelley's paper[2] and Deissler and Perlmutter's one[3] are remarkable as theoretical studies about energy separation, but the starting point of these papers differs from the true conditions.

The authors measured velocity and energy distributions of vortex flow in the tube under several different conditions; and made clear the relations of energy separation and flow profile, and the influences of size factors and working conditions on them; convenient size factors were introduced here to sum up the results.

II. Nomenclature

$a=\sqrt{\kappa g R T}$; sound velocity (m/s)
$D=2R$: inner diameter of tube (mm)
d_n : nozzle diameter (mm)
d_0 : diameter of cold end orifice (mm)
E : quantity of energy flow per unit time (kcal/s)
G : quantity of mass flow per unit time (kg/s)
g : gravitational acceleration (m/s^2)
$\kappa=C_p/C_v$: ratio of the specific heat (at constant press. and constant volume)
L : distance from nozzle center along the axis of tube (mm)
$M=v/a$: Mach number

$M_n = v_n/a_n$: Mach number of jet flow from nozzle
p : pressure (mm Hg abs.)
$R(=D/2)$: gas constant (or tube radius) ($m/°K$ or mm)
r : radius (mm)
T : absolute temperature ($°K$)
v : flow velocity (m/s)
v_0 : peripheral component of flow velocity (m/s)
v_z : axial component of flow velocity (m/s)
v_r : radial component of flow velocity (m/s)
v_n : flow velocity at nozzle opening (m/s)
$\alpha = \mathrm{Tan}^{-1}(v_z/v_0)$: flow angle (°)
γ : specific weight of gas (kg/m³)
G_c : quantity of cold air flow per unit time (kg/s)
G_h : quantity of hot air flow per unit time (kg/s)
G_t : quantity of total air flow per unit time (kg/s)
ξ : G_c/G_t
η : efficiency

III. Apparatus and Method of Experiment

(1) Fig. 1 shows a schematic view of apparatus. Compressed air enters into a surge tank, where pulsative flow changes to stationary stable one, cooled to constant temperature through an intercooler, then passes a filter of glass wool to become dry clean air, then the air flows out of nozzles tangentially along the outer radii of the vortex tube, and the air is divided into hot part and cold one. The quantity of total air flow is measured by the standard pipe orifice 1. Both hot air and cold one has peripheral velocity component, so it is diminished by the rectifiers 2 and 3, then by the pipe orifices 4 and 5 we measured the quantity of air flow, and calculated the ratio of quantity of air flow ξ. The ratio ξ is adjusted by the valve 6. Tube length of the vortex tube apparatus was made long

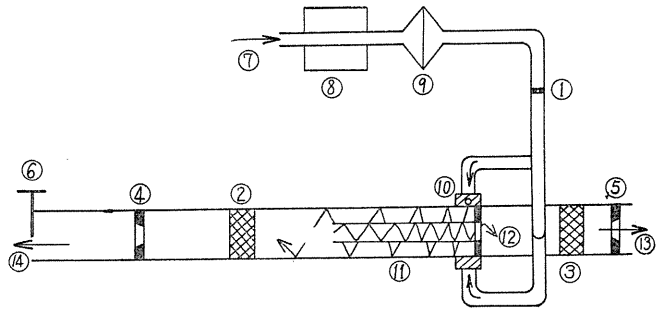

1, 4, 5: standard pipe orifices
2, 3: rectifiers
6: sluice valve
7: compressed air from surge tank
8: cooler
9: filter of glass wool
10: nozzles
11: plastic tube, about 8.5 m long
12: cold end orifice
13: cold air
14: hot air

FIG. 1, chematic view of apparatus

enough considering the results of preparatory experiments; the tube was made of plastic to avoid heat loss. In the case of 2″ pipe experiments we used a transparent plastic tube and made a visualization study by silk to get the outline of flow pattern.

(2) Fig. 2 shows a vortex chamber and a cold end orifice for the inner diameter of tube $D=52.8$ mm (2″). Almost the same in the case of $D=78$ mm (3″). Table (1) shows each nozzle and Table (2) shows the size of cold end orifices. We refered to Ôno and Taniguchi's paper[4] for selection of the size.

TABLE 1. Size of Nozzles

Inner dia. of tube D (mm) (inch)	Nozzle dia. d_n (mm)	No. of nozzle z	d_n/D	$z(d_n/D)^2$
78.0(3)	11.0	2	0.141	0.0398
78.0(3)	9.0	2	0.115	0.0266
52.8(2)	11.0	2	0.217	0.0870
52.8(2)	9.0	2	0.171	0.0582
52.8(2)	6.5	2	0.123	0.0304
52.8(2)	9.0*	2	0.171	0.0582

* Nozzle inclined against hot end 8°

TABLE 2. Size of Cold End Orifices

For tubes $D=78.0$ mm (3″)		For tubes $D=52.8$ mm (2″)	
Hole dia. of orifice d_0 (mm)	d_0/D	Hole dia. of orifice d_0 (mm)	d_0/D
45.45	0.581	30.3	0.574
39.78	0.510	26.52	0.502
34.5	0.443	23.0	0.436
23.0	0.295	18.9	0.358
—	—	13.0	0.246
0	0	0	0

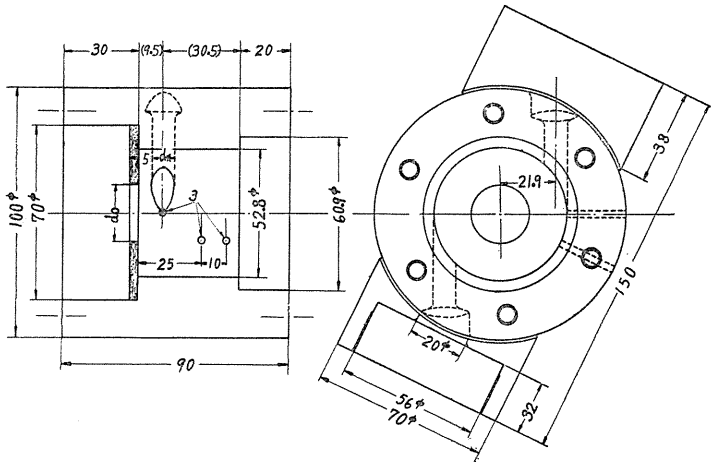

FIG. 2. Vortex chamber and cold end orifice for inner diameter of tube $D=52.8$ mm.

(3) Cylinder type Pitot tubes and stagnation temperature probes as shown in Fig. 3 were used to measure flow angle, pressure and stagnation temperature of air flow in the tube. Measurement of stagnation temperature, flow angle, stagnation and static pressure was made in a few section for each combination of nozzle diameters and cold end orifice diameters.

We measured these values in the plane of nozzle center ($L/D=0$) by Pitot tubes and stagnation temperature probes penetrating axially through cold end orifices. The pressure probe *c* and the stagnation temperature probe *f* were used for the central core region. We first used the 5 holes-sphere-type Pitot tube *a* to measure values in several sections except the nozzle section. This showed that radial velocity component is negligible.

We decided to use the cylinder type Pitot tube to measure values in each section. Calibration results of the Pitot tube are shown in Fig. 4. Fig. 5 shows recovery factor calculated by the data of jet from the tank nozzle[5].

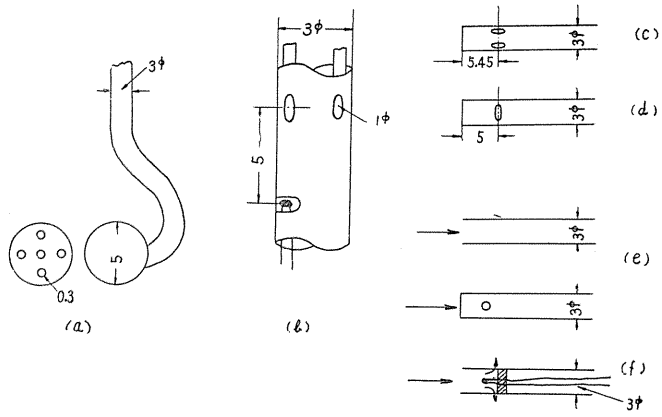

FIG. 3. Pitot tubes and stangnation temperature probes

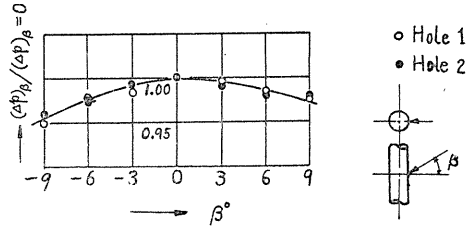

FIG. 4. Calibration results of Pitot tube (FIG. 3 (*b*)).

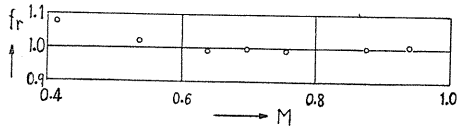

FIG. 5. Recovery factors of stagnation temperature probe (FIG. 3 (*b*)).

IV. Results

Stagnation pressure p_0, static pressure p, flow angle α and total temperature T_0 were measured in several sections for the apparatus of different pipe diameters and different nozzle diameters. Mach number M and static temperature T were calculated by the next formula[6],

$$p_0/p = \left(1+\frac{\kappa-1}{2}M^2\right)^{\kappa/\kappa-1} \tag{1}$$

and

$$T_0/T = \left(1+\frac{\kappa-1}{2}M^2\right). \tag{2}$$

We calculated sound velocity $a=\sqrt{\kappa gRT}$, flow velocity $v=Ma$ and axial velocity component $v_z=v\cdot\sin\alpha$. In the case of central region, we neglected compressibility of air for calculation. We measured nozzle inlet pressure at the tube wall just before the nozzls, and nozzle outet pressure through a hole situated at the tube wall just after the nozzle. The mach number of jet flow M_n, jet flow velocity v_n and adiabatic temperature drop $(\Delta T)_n$ were introduced, assuming isentropic expansion in the nozzle from inlet pressure p_n to exit pressure p. The distribution of Mach number and flow velocity at each section of the tube were shown as ratios with M_n and v_n respectively. The increase or decrease in total temperature and static temperature is shown in figure as values divided by $(\Delta T)_n$.

(*1*) *Velocity distribution of air flow* (Fig. 6-8)

Fig. 6, 7 and 8 show Mach number (M/M_n), tangential velocity component (v_θ/v_n), and axial velocity component (v_z/v_n) introduced from the results measured in detail for the four sections $L/D=0$ (where the nozzle center is located), $L/D=0.5$, 3 and 13. Nondimensional radius r/R was used as the axis of abscissa, where r is radius at measuring position and R is inner tube radius.

(*2*) *Diameter of core* (Fig. 9 and 10)

The radius at boundary of counterflow r_c changes according to nozzle size

Symbols for Fig. 6~Fig. 9 and Fig. 11~Fig. 13.

	D mm	dn mm	z	d_n/D	M_n
□	78	11	2	0.141	0.8
■	78	9	2	0.115	1
×	52.8	11	2	0.215	0.65
△ ▲	52.8	9	2	0.171	0.8 0.5
●*	52.8	9.2	2	0.174	0.8
○ ◑*	52.8	9	2	0.171	0.8 0.5
※	52.8	6.5	2	0.171	1

* Nozzle inclined (8°)

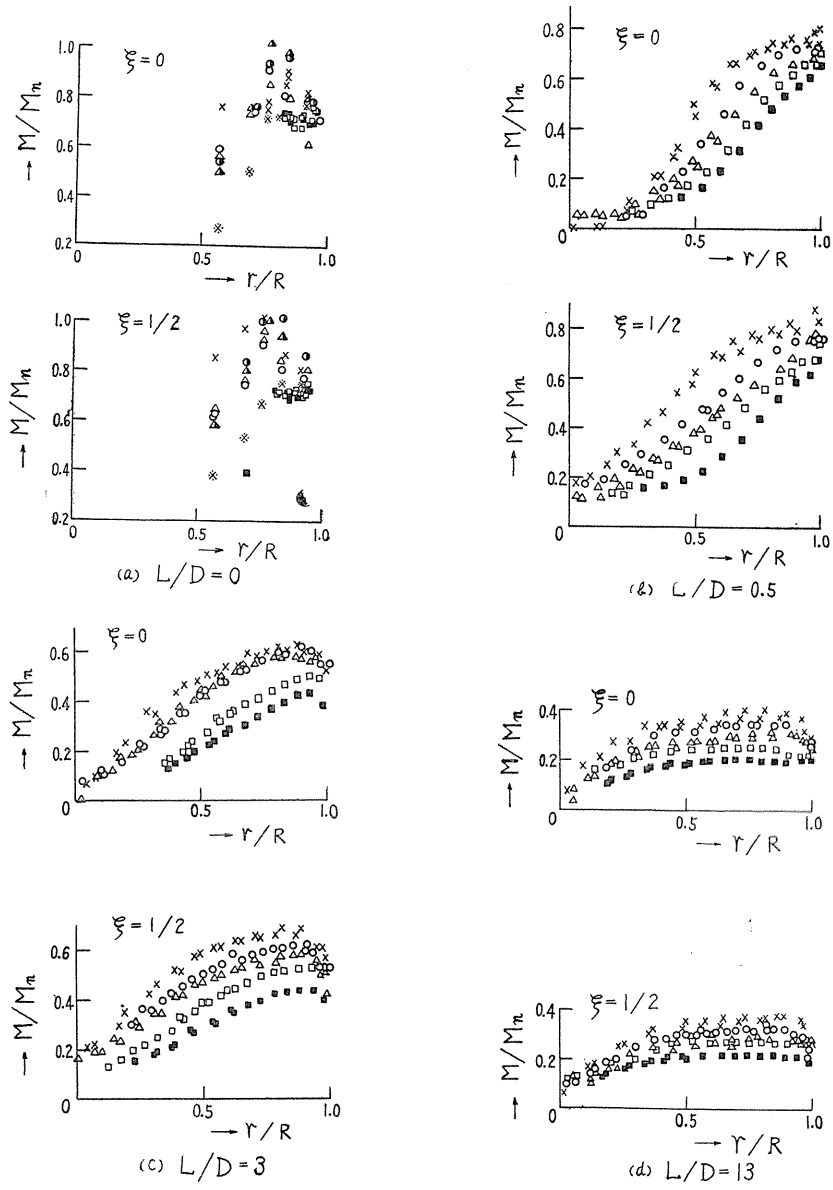

FIG. 6. Distribution of mach numbers in four sections.

(d_n/D) as shown in Fig. 9. It also changes according to cold end orifice diameter (d_0/D) as shown in Fig. 10. We measured r_c at many sections, and all the data are shown in the figures.

(3) *Distribution of flow angle* (Fig. 11)

The distribution of flow angle at the three sections L/D=0.5, 3 and 13 are shown in Fig. 11 (a), (b) and (c) respectively. Experimental error for flow angle is extremely small, less than 0.2 degrees.

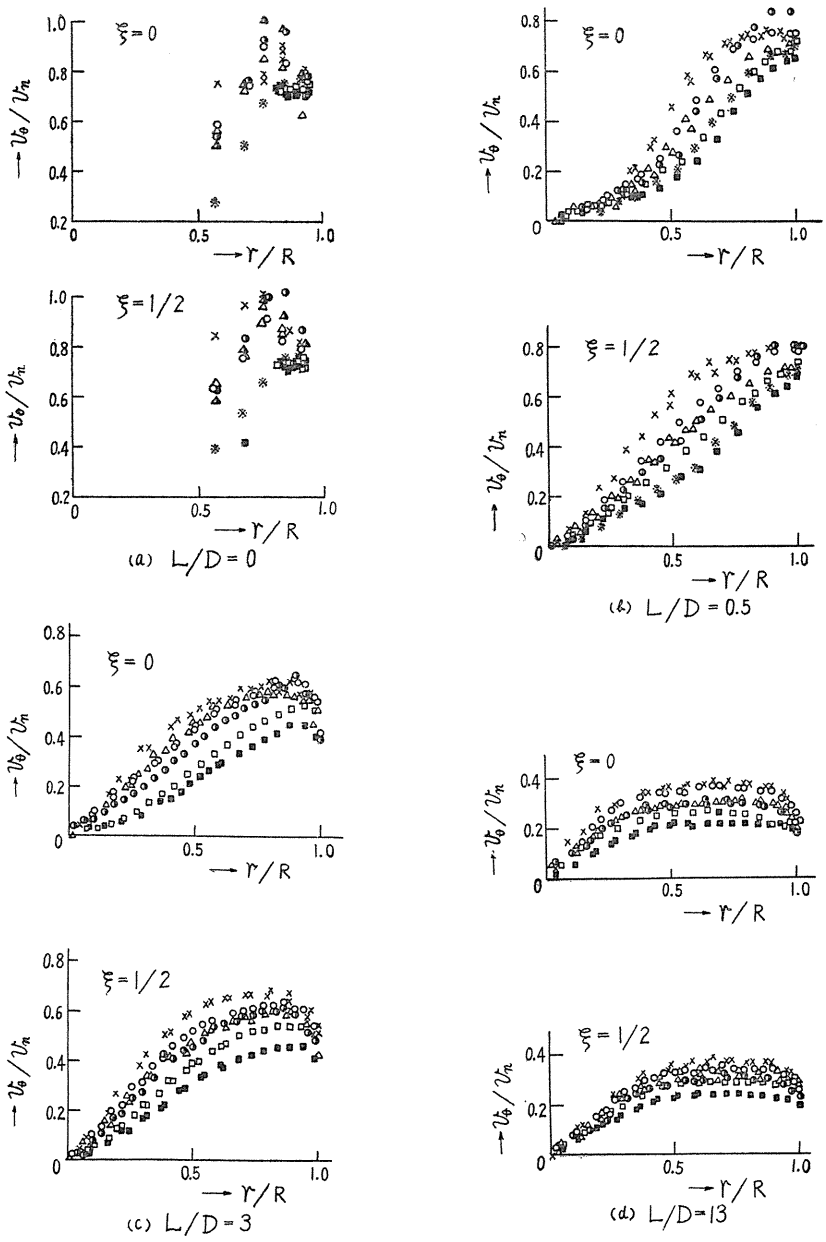

FIG. 7. Distribution of tangential velocity components in four sections.

(4) *Distribution of stagnation temperature* (Fig. 12)

The distribution of stagnation temperature at the four sections $L/D=0$, 0.5, 3 and 13 are shown in Fig. 12 (a), (b), (c) and (d) respectively. Although there exist gradients of total and static temperature refering to radius, the authors are sure through another preparatory experiment that no error enters into stagnation

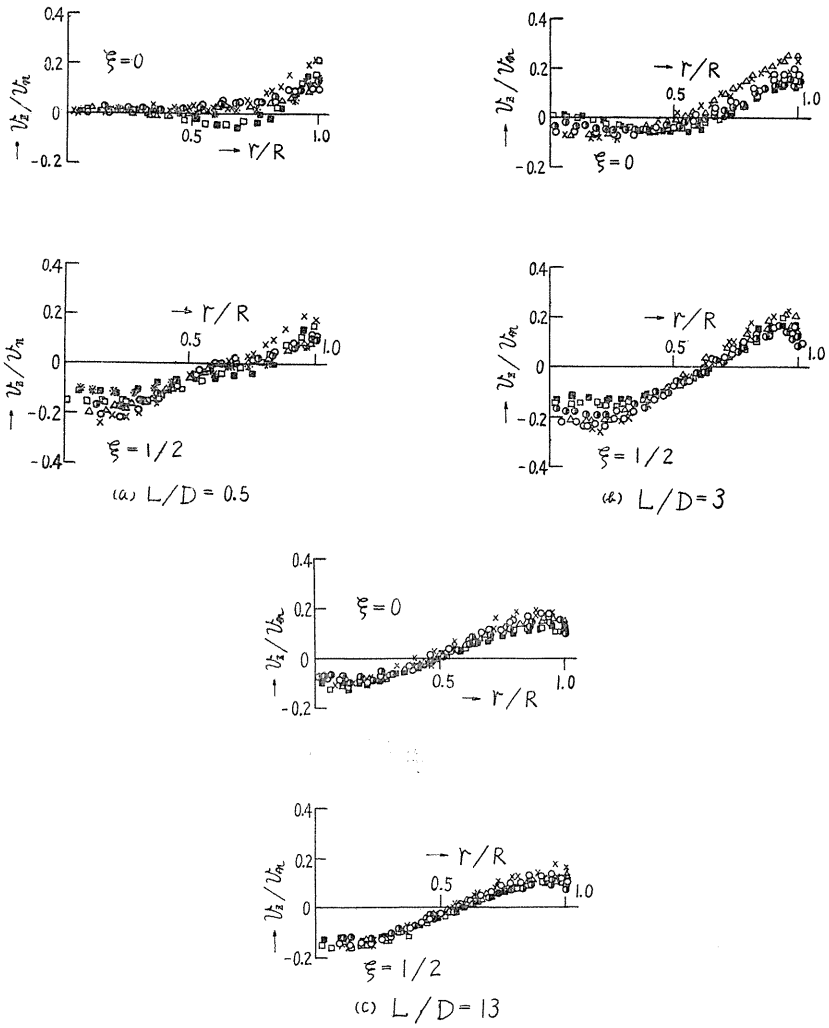

FIG. 8. Distribution of axial velocity components in three sections.

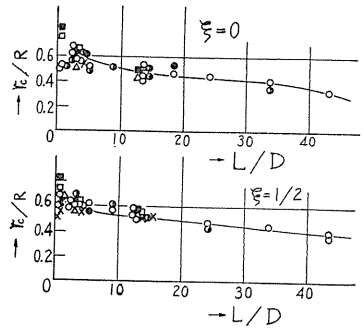

	D_{mm}	d_n mm	Z	d_n/D	Mn
□	78	11	2	0.141	0.8
▩	78	9	2	0.115	1
×	52.8	11	2	0.215	0.65
△	〃	9	2	0.171	0.8 0.5
◍*	〃	9.2	2	0.174	0.8
○*	〃	9	2	0.171	0.8 0.5
※	〃	6.5	2	0.171	1

* Inclined nozzle (8°)

FIG. 9. Changes of diameter of core according to nozzle size (d_n/D).

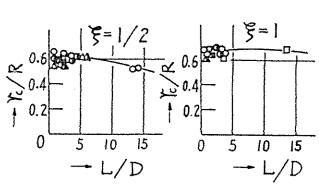

	d_0	M_n
○	23	0.8
◉	23	0.5
□	18.9	0.8
▣	18.9	0.5
△	13	0.8
▲	13	0.5

FIG. 10. Changes of diameter of core according to cold end orifice diameter (d_0/D) (D=52.8 mm(2″), d_n=9 mm).

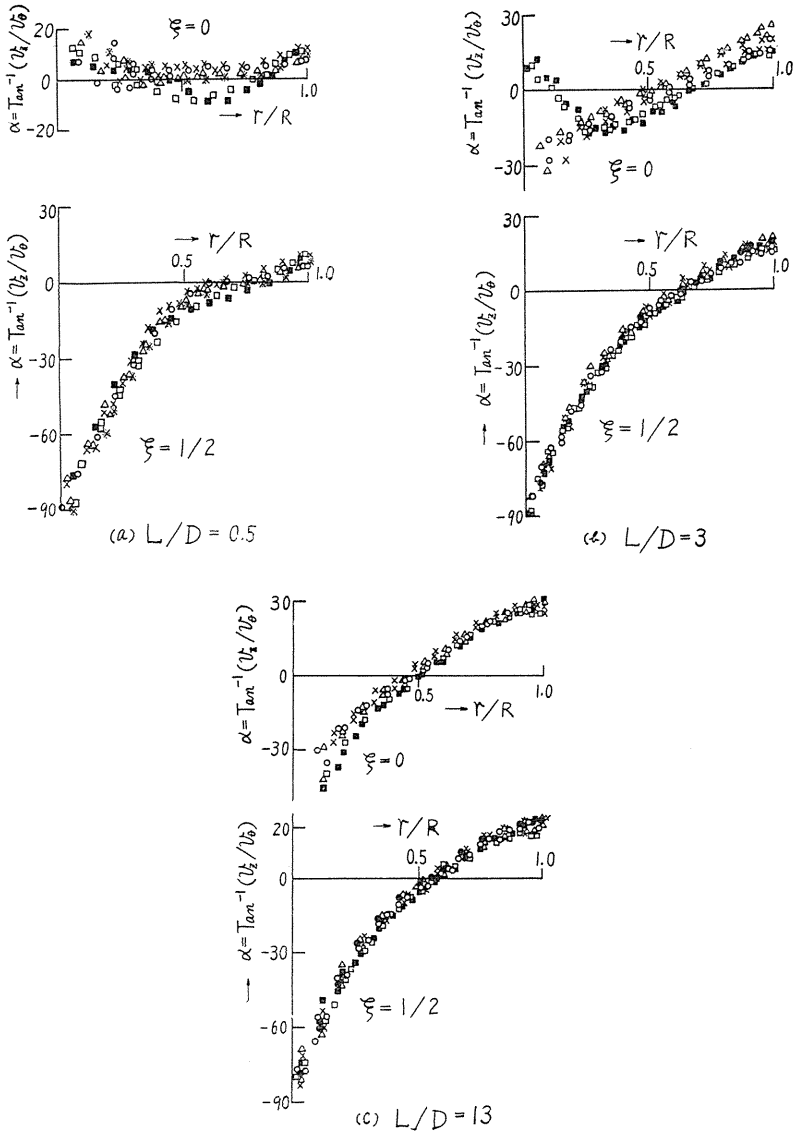

FIG. 11. Distribution of flow angles in three sections.

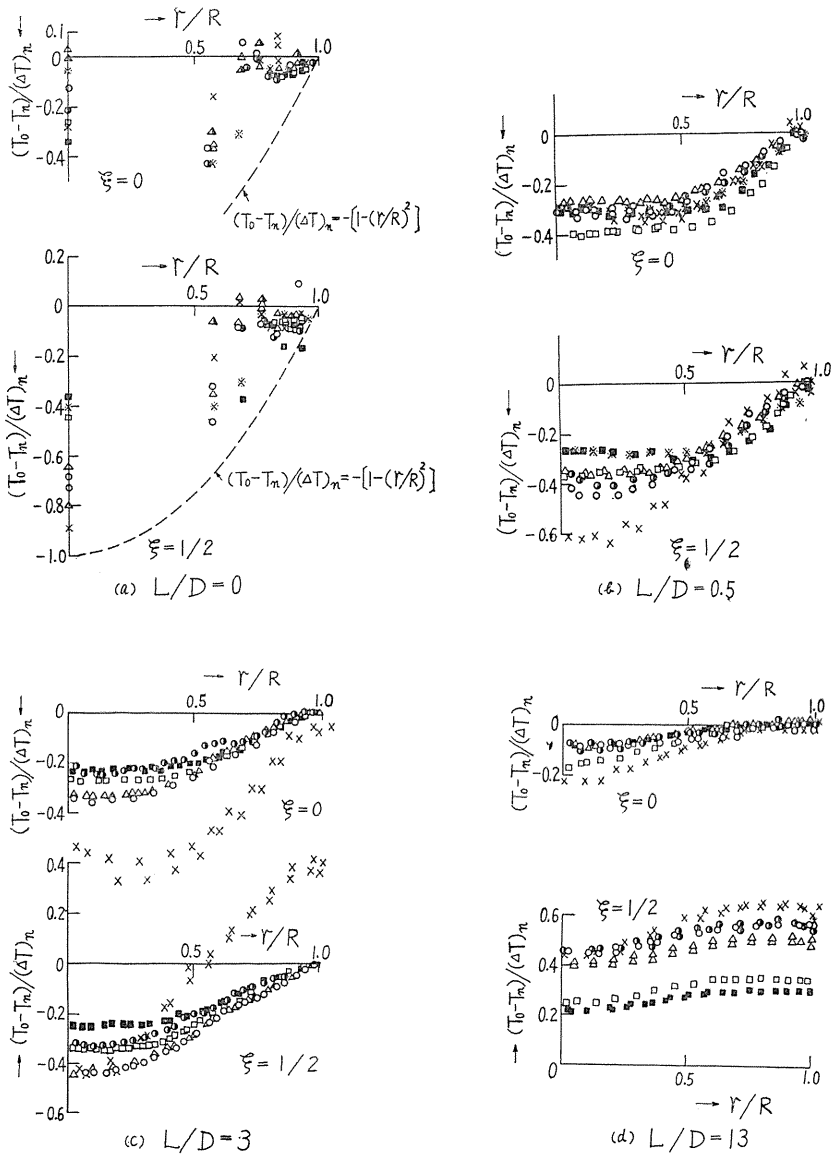

FIG. 12. Distribution of stagnation temperatures in four sections.

temperature if they measure it by the probe traversing a tube along its diameter. Stagnation temperature shown here, therefore, has little error.

(5) *Distribution of static temperature* (Fig. 13)

The distribution of static temperature calculated for the four sections were shown in Fig. 13. Errors of static temperature, as composed of errors of pressure and stagnation temperature, are more than those of stagnation temperature, but they are less than 2 or 3 percent.

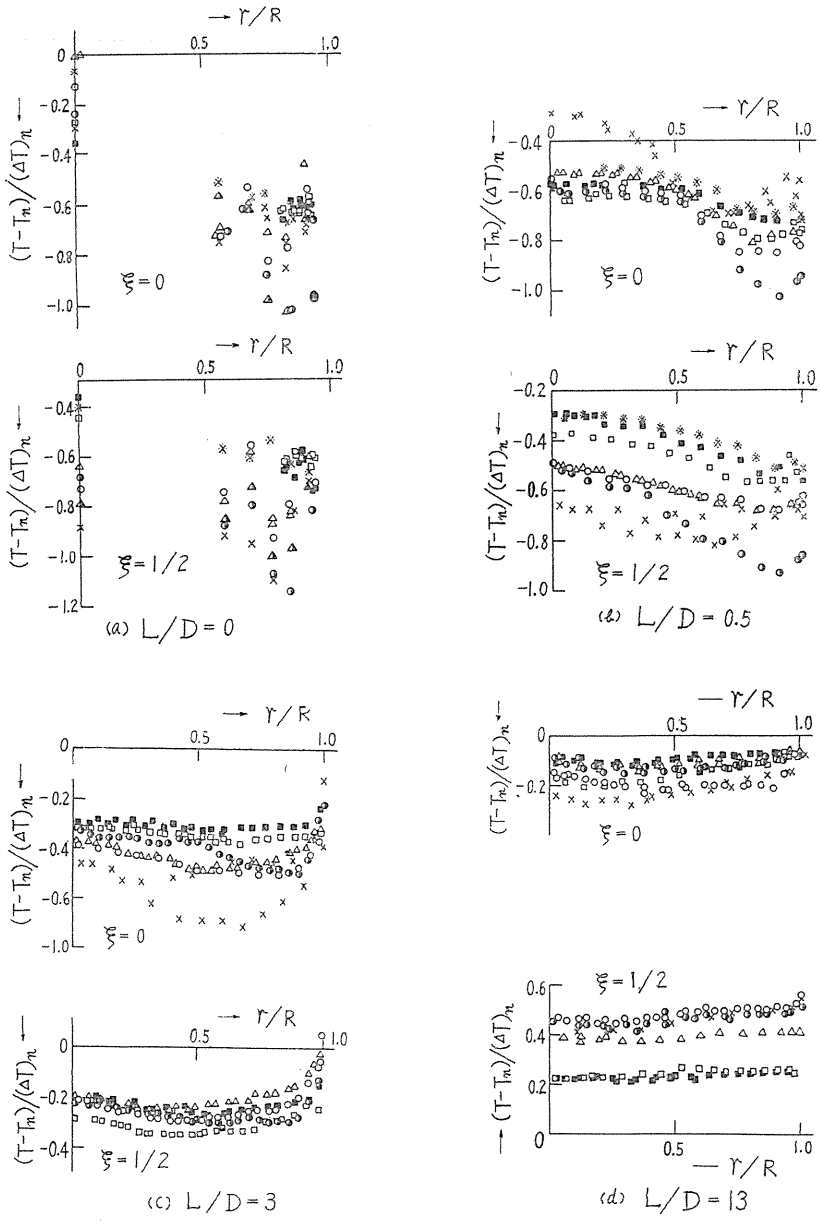

FIG. 13. Distribution of static temeratures in four sections.

V. Discussion

We pointed out that the flow angle α has extremely small error, but in Fig. 11 it seems that there exists rather large error in the value. As the reason for it small fluctuation of the vortex flow itself is to be pointed out; the fluctuation is due to small pressure deviation in compressed air even under very cautious

adjustment, where happens freezing sometimes at nozzle exits. As our experiment was not carried out under conditions of fully peripheral discharge but partially peripheral discharge, the axially symmetric flow did not fully develop near nozzle exits, and therefore the values measured at $r=r_k$ and $r=-r_k$ are different. But it is not so far from symmetry, and the symmetric flow fully developed in the section $L/D=3$. Strong vibration of air in full tube appears in the case of flow ratio $\xi>3/4$. There did not appear strong vibration under the conditions of our measurements. Considering these points each datum has superposed errors based on several factors. But they are not so large, and these results play assuredly the very sole for analysis.

(1) Flow velocity

The air flowing out of nozzles into the tube goes down against the hot end orifice (leftwards in Fig. 1), then it revolves with very high speed near the tube wall tangentially. According to this vortex, there exists low (sometimes negative) pressure in the central part of the tube. By the suction of this low pressure there appears back flow towards the cold end orifice (in Fig. 1 towards right) in the center of the tube. This back flow interferes or mixes with the main flow in the outer part at the core boundary, when the flow in the inner region gains revolutional motion by shearing.

As shown in Fig. 6, Mach number of each section is large in the vortex chamber which has large specific crossectional area of the nozzle openings $(d_n/D)^2 \cdot z$.

Near the nozzle where L/D is small, M/M_n is larger for larger flow ratio ξ. This is apparently due to axial velocity.

Direction of the axial velocity component v_z/v_n in the back flow region is, as seen in Fig. 8, different from that in the outer annular region. As the back flow in the center of tube stagnates at the diaphragm when $\xi=0$, v_z/v_n around the center becomes smaller gradually on its approaching to the nozzle section, but at the section far from the nozzle it does not differ from that in the case of $\xi>0$.

In the annular region, distribution of v_z/v_n is hardly influenced by the flow ratio ξ and the larger $(d_n/D)^2 \cdot z$ is, the larger v_z/v_n is; $\partial v_z/\partial r$ is nearly constant when L/D is small; on the other hand when L/D becomes large, the boundary layer of tube wall develops. The absolute values $|v_z|$ of back flow at the center become small when L/D becomes large and they approach to zero for comparatively large value of L/D. For larger L/D, the back flow diminishes and axial velocity at each radius reaches the mean value. We neglected to show the result of preparatory experiment treating these criteria.

It is clearly seen from the experimental results that the tangential velocity component v_θ/v_n is a main, important factor affecting total temperature distribution. The value v_θ/v_n is larger for large $(d_n/D)^2 \cdot z$. In the back flow region, it has the larger value when $\xi=1/2$ than when $\xi=0$ at the section near nozzles. When $L/D=0$ the velocity (v_θ/v_n) in the annular region corresponding to nozzle openings is uniform, and in the back flow region angular velocity is constant. As L/D becomes comparatively large, the distribution of v_θ/v_n in the section is almost the same as that of perfect forced vortex. When L/D becomes larger its distribution near the tube wall resembles to that of free vortex.

(2) *Back flow*

As seen from the distribution pattern of flow angle α or axial velocity v_z, two annular boundaries appear when $\xi=0$, and the air in the annular region enclosed with these boundaries flows backwards. For $\xi>0$ there appears single cylindrical back flow region in the center of tube. The radius of boundary of the back flow region or core r_c/R is larger when ξ becomes larger in comparison with that for $\xi=0$. It depends on pushing force of the back flow. According to the authors' experiment r_c/R for smaller quantity of total air ($G_t=30$ g/s) is rather small as compared with that for larger one ($G_t=60$ g/s). We conclude the radius r_c/R is not so influenced by the change of G_t of this order. For the small area of nozzle openings $(d_n/D)^2z$, r_c/R is larger than for larger one; this effect is specially remarkable just after nozzle openings. This shows that the quantity of jet flow from nozzles has main influence on r_c/R.

Concerning with the radius of cold end orifice (d_0/D), it is said that r/R is larger for large (d_0/D), this effect is remarkable near the nozzles. When (d_0/D) is too large, flow of the outer region near the cold end orifice is influenced and separation effect diminishes. It is considered that the air down the cold end orifice is suctioned by too low pressure of the inner region. Diminishing (d_0/D) has no bad effect on the energy or mass separation.

(3) *Flow angle*

Flow angle α is influenced by the value $(d_n/D)^2\cdot z$ near the nozzle, but the influence is not so clear for large L/D.

As axial velocity distribution of the section near nozzle for large radius is linear (Fig. 8 (a)), we put

$$v_z/v_n=b(r-r_c)/(R-r_c). \tag{3}$$

The assumption that the air from the nozzle does not flow into the central back flow region before this section, if we neglect compressibility of air, leads us to the following from the continuity equation:

$$\begin{aligned} & z\frac{\pi d_n^2}{4}\cdot v_n=\int_{r_c}^{R}2\pi r dr\cdot b\frac{r-r_c}{R-r_c}v_n \\ \therefore\quad & zd_n^2=\frac{8b}{R-r_c}\left[R^2\left(\frac{R}{3}-\frac{r_c}{2}\right)+\frac{r_c^3}{6}\right] \\ & z\left(\frac{d_n}{R}\right)^2=\frac{8b}{1-\frac{r_c}{R}}\left[\frac{1}{3}-\frac{1}{2}\left(\frac{r_c}{R}\right)+\frac{1}{6}\left(\frac{r_c}{R}\right)^3\right] \end{aligned} \tag{4}$$

We calculate b from the equation (4), and from the equation (3) it follows $(v_z/v_n)_{r=R}=b$. Accordingly flow angle at the tube wall $\alpha_{r=R}$ is calculated as follows:

$$\alpha_{r=R}=\mathrm{Sin}^{-1}(v_z/v_n)_{r=R}=\mathrm{Sin}^{-1}b \tag{5}$$

Calculated results agree well with experimental data as shown in Table 3. From this fact we see that α for large area of nozzle openings is large, and we see how large it is.

(4) *Stagnation temperature*

Comparison of Fig. 7 with Fig. 10 shows that stagnation temperature distri-

TABLE 3. Examples of $\alpha_{r=R}$

$z(d_n/D)^2$	D mm(inch)	d_n (mm)	z	r_c/R	ξ	$\alpha_{r=R}$ Calculated	$\alpha_{r=R}$ Experimental	Experimenter
0.058	52.8(2)	9	2	0.68	1/2	11°49′	8°	The authors
0.087	52.8(2)	11	2	0.58	1/2	15°08′	13°	
0.040	78.0(3)	11	2	0.75	1/2	10°04′	12°	
0.125	78.0(3)	9.8	8	0.60	0	21°09′	21°~22°	Hartnett and eckert

bution corresponds to tangential velocity distribution. Apparatus of large $(d_n/D)^2 \cdot z$ has large $\partial T_0/\partial r$ and $\partial T_0/\partial r$ is larger for faster jet velocity of the same apparatus. For larger angular momentum around the tube center of jet flow from nozzle, forced vortex grows up completely and $\partial\left(\frac{\gamma}{2g}v_0^2\right)/\partial r$ is large—that is $\partial T_0/\partial r$ grows large. All the same for larger quantity of air.

For $\xi=0$, T_0 is nearly equal to T_n in the outer region, and in the back flow region T_0 is rather small in comparison with T_n for small L/D. When L/D becomes larger, then it grows large. Finally $T_0=T_n$ for all over the section. For $\xi>0$ T_0 of the outer region is nearly equal to T_n for the first time, and it grows larger than T_n for larger L/D. This is due to the fact that particles of low energy level separate gradually and fall into the back flow region.

The value T_0 is more influenced for $\xi>0$ than for $\xi=0$ by area of nozzle openings, quantity of air and so on. Nozzles with a slight angle to peripheral direction separates mass or energy well.

(5) *Static temperature*

For jet flow from nozzles static temperature seems to be the value corresponding to adiabatic heat drop in nozzles, but experimental results show that for the value $L/D=0.5$ static temperature already becomes high. This is due to both skin friction at the tube wall and internal friction.

For each section pattern of the distribution of temperature is not so influenced by air quantity and $(d_n/D)^2 \cdot z$. For small L/D, $|\partial T/\partial r|$ is large and temperature is higher in the central portion than in the outer region. This is brought up by the back flow air suctioned constantly into the portion. And temperature difference between the back flow and the main one appears. However, as the contact area of the back flow and the main one is small and tempcrature difference is not so large, and the heat transferred seems to be so small.

(6) *Changes of some properties along tube axis* (Fig. 14)

(a) Quantity of air flow (Fig 14 (a))

The quantity of air flow of the outer region and the inner back flow region is calculated from

$$\left.\begin{aligned} G_I &= \int_{r_c}^{R} \gamma \cdot v_z \cdot 2\pi r dr \\ G_{II} &= \int_{0}^{r_c} \gamma \cdot v_z \cdot 2\pi r dr \end{aligned}\right\} \tag{6}$$

with axial velocity v_z and specific weight γ at each measured point.

There is an example of calculated result of G_I/G_h, G_{II}/G_c and $(G_I-G_{II})/G_h$ in Fig. 14 (a). The air quantity of back flow region increases to G_c as it approaches to the cold end orifice. The air quantity of main flow in the outer annular region first is G_t, gradually decreases to G_h. Low energy particles fall into the back flow region. $(G_I-G_{II})/G_h$ is theoretically a unity, but the results show error less than 5%, The sharp gradient of G_I, G_{II} to z appears near the section of $L/D=13$ as shown in the figure, but the calculated result of radial velocity $v_r=-dG_{II}/(\gamma\cdot 2\pi r_c\cdot dz)=0.5\sim1.0$ m/s. Therefore, v_r is negligible small in comparison with v_0 and v_z.

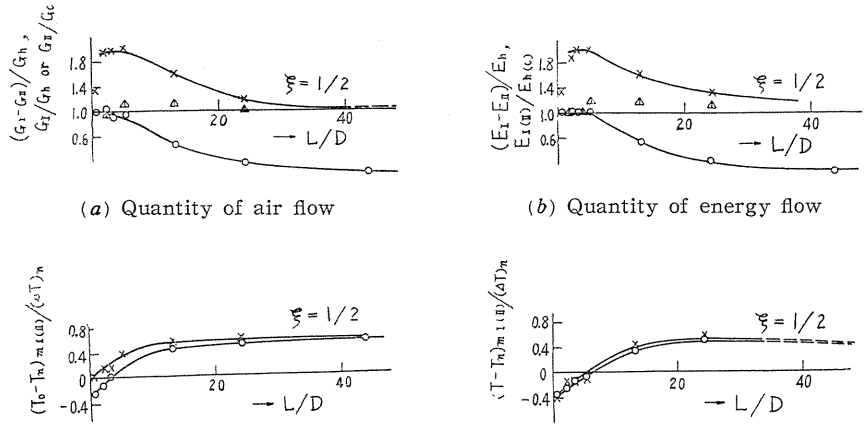

(*a*) Quantity of air flow (*b*) Quantity of energy flow

(*c*) Mean stagnation temperature (*d*) Mean static temperature

× Main flow ○ Back flow △ Error in experiment

FIG. 14. Changes of some properties along tube axis ($D=52.8$ mm, $d_n=9$ mm and inclined nozzle).

(b) Quantity of energy flow (Fig. 14 (b))

As well as the quantity of air flow, we calculated the quantity of energy flow of the outer region and the inner back flow region by the following;

$$\left.\begin{aligned} E_I &= \int_{r_c}^{R} C_p T_0 \gamma v_z \cdot 2\pi r dr \\ E_{II} &= \int_{0}^{r_c} C_p T_0 \gamma v_z \cdot 2\pi r dr \end{aligned}\right\} \tag{7}$$

and showed E_I/E_h, E_{II}/E_c and $(E_I-E_{II})/E_h$ in Fig. 14 (b).

It is clearly seen that the energy flow pattern corresponds to the mass flow pattern. In the back flow region E_{II} increases as L/D decreases and the quantity of decrease in E_I is due to the quantity of increase in E_{II}. In the case of energy, however, as low energy particles fall into the back flow region, the increase of total quantity of energy flow in the back flow region (E_{II}) brings the decrease of its mean energy or mean stagnation temperature.

(c) Mean value of stagnation temperature (Fig. 14 (c))

The quantity of energy flow of each section is not enough to explain the

energy separation mechanism, so the authors calculated the mean stagnation temperature from the next equations and showed in Fig. 14 (c).

$$\left.\begin{aligned}(T_0-T_n)_{Im}&=\left[\int_{r_c}^{R}\gamma v_z\cdot 2\pi r C_p(T_0-T_n)dr\right]/C_pG_I\\(T_0-T_n)_{IIm}&=\left[\int_{0}^{r_c}\gamma v_z\cdot 2\pi r C_p(T_0-T_n)dr\right]/C_pG_{II}\end{aligned}\right\}\qquad(8)$$

The figure shows clearly that the stagnation temperature T_0 of the outer region approaches to T_h, and that of the back flow region to T_c. $(T_0-T_n)_{Im}>(T_0-T_n)_{IIm}$ for each section. As shown in the figure mean stagnation temperature saturates to T_h as L/D becomes large; there is a certain length of tube, by which the performance of the vortex tube apparatus is not so influenced.

The authers installed flow rectifiers in the pipe actually to diminish vortex and eddies. This assuredly showed that for $L/D=10\sim15$ efficiency or performance is almost the same as for $L/D\gg10$.

(d) Mean static temperature (Fig. 14 (d))

As well as stagnation temerature, we calculated mean static temperature by the following:

$$\left.\begin{aligned}(T-T_n)_{Im}&=\left[\int_{r_c}^{R}\gamma v_z\cdot 2\pi r C_p(T-T_n)dr\right]/C_pG_I\\(T-T_n)_{IIm}&=\left[\int_{0}^{r_c}\gamma v_z\cdot 2\pi r C_p)T-T_n)dr\right]/C_pG_{II}\end{aligned}\right\}\qquad(9)$$

and showed in Fig. 14 (d). The distribution pattern resembles to that of stagnation temperature, but there is a region of higher temperature in the inner region than in the outer region.

(7) *Performance* (Fig. 15)

To see the accuracy of experimental heat loss rate of the apparatus, η_{loss} is calculated for all experiments by the following:

$$\eta_{loss}=[\xi T_c+(1-\xi)T_h]/T_n\qquad(10)$$

and it is clearly shown that the error is less than one percent. To compare the performances we introduced two kinds of efficiencies. One is efficiency η_{iso} due to isothermal compression, defined as to use both hot air and cold air; the other is efficiency η_{ad} due to adiabatic compression, defined as to use cold air only. Fig. 15 shows these calculated values.

$$\eta_{iso}=\frac{\kappa}{\kappa-1}\cdot\frac{\xi(T_n-T_c)+(1-\xi)(T_h-T_n)}{T_n\ln(p_n/p_a)}\qquad(11)$$

$$\eta_{ad}=\frac{\xi(T_n-T_c)}{T_n-T_{na}},\qquad(12)$$

where p_a=atm. pressure, $T_{na}=T_n(p_a/p_n)^{\kappa-1/\kappa}$.

The efficiencies η_{iso} and η_{ad} take the value zero for $\xi=0$ and $\xi=1$; and the maximum value for $\xi=1/2\sim2/3$. The graph shows the values for $\xi=1/2$,

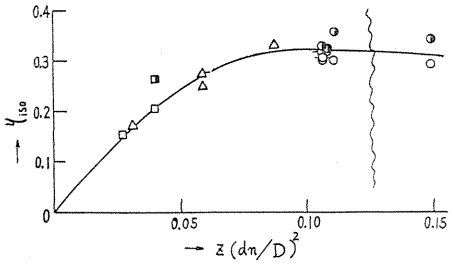

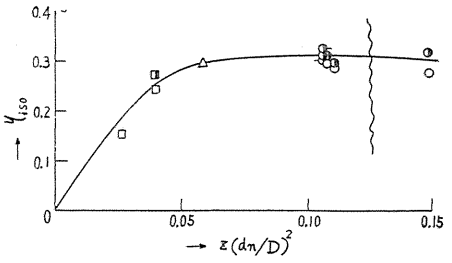

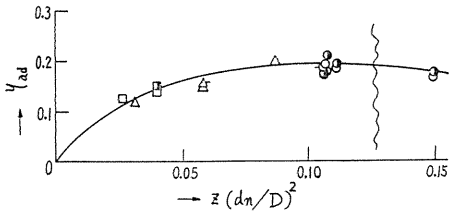

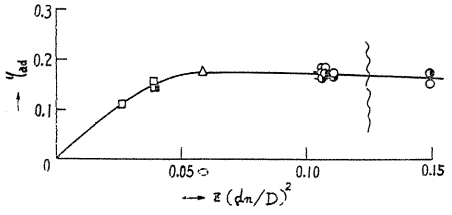

	D mm	Nozzle inclination	M_n
□	78	0°	1
◧	78	0°	0.5
△	52.8	0°	1
△-	52.8	8°	1
○	27.6	0°	1
◑	27.6	0°	0.5
○-	27.6	8°	1
◑-	27.6	8°	0.5

(*a*) Effect of nozzle opening on performance when $\xi=1/2$ and $d_0/D=0.436\sim0.44$.

	D mm	Nozzle inclihnatin	M_n
□	78	0°	1
◧	78	0°	0.5
△	52.8	0°	1
○	27.6	0°	1
◑	27.6	0°	0.5
○-	27.6	8°	1
◑-	27.6	8°	0.5

(*b*) Effect of nozzle opening on performance when $\xi=1/2$ and $d_0/D=0.574\sim0.581$.

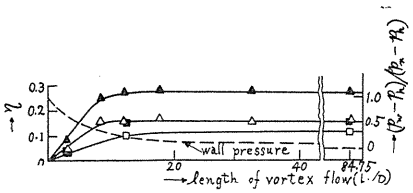

p_h = Wall pressure before hot end orifice
p_n = Wall pressure before nozzles
p_w = Wall pressure at any potnt

	Efficiency	D mm	d_n mm	Nozzle inclination	d_0
▲ △	η_{iso} η_{ad}	52.8	9	8°	23.0
■ □	η_{iso} η_{ad}	78	9	0°	45.45

(*c*) Effect of length of vortex flow on performance ($\xi=1/2$).

FIG. 15. Performance

(a) Effect of $(d_n/D)^2 \cdot z$

As already mentioned $\partial T_0/\partial r$ becomes larger for large $(d_n/D)^2 \cdot z$. Therefore both η_{iso} and η_{ad} are large in the case.

However, the efficiencies do not increase more for larger value $(d_n/D)^2 \cdot z$ than for the value of one of the apparatus we used, of which D is 52.8 mm, d_n is 11 mm and z is 2. This is surely shown by additional experiments with the apparatus of 27.6 mm (1″) tubes.

(b) Effect of (d_0/D)

For small diameters of the cold end orifice the discharge coefficients of cold air decrease, that is the discharge resistance of cold air increases. Accordingly the efficiencies become very bad. On the other hand, for too large d_0, the efficiency decreases as well. It is because of the straight short cut discharge of main flow to the cold end, and the suction due to large negative pressure in the center. Generally speaking, the efficiencies are almost constant for the range of $d_0/D=0.45\sim0.55$, and upper limit of d_0/D is 0.6. This value corresponds to core radius.

(c) Length of vortex core or tube

As shown in Fig. 15 (c) the vortex tube for $L/D=20$ is long enough to get saturated high efficiency.

VI. Conclusion

(1) Energy separation in the vortex tube refers to the distribution pattern of peripheral velocity component.

(2) Energy separation is quickened by the perfect forced vortex, in the case of enough angular momentum around the tube axis of jet at the exit of nozzle.

(3) Even in the case of the same jet velocity, the temperature difference between hot air and cold air for smaller tube diameter (that is, for larger angular velocity) is larger. However, the difference in efficiencies between smaller tube diameters and larger tube diameters is small.

(4) Few energy differences exist within the back flow region. Remarkable energy difference appears within the annular boundary layer between main flow and back flow.

Mechanism of energy separation is explained by molecular turbulences within the boundary.

(5) Nondimensional expression of velocity and temperature explains the main factors influencing on energy separation in the vortex tube.

(6) The authors think that nozzle efficiency, separation efficiency etc. should be introduced in regard to efficiencies. It is better to divide efficiency into these unit efficiencies.

VII. Acknowledgement

The authors express their appreciations to Professor Dr. A. Kobayashi and Professor Dr. Y. Furuya of Nagoya University for their encouragement and guidance throughout this research and to Professor Dr. K. Iinoya of Nagoya University and Professor Dr. M. Murakami of Osaka City University for their valuable advices.

The authors are due to express their thanks to Mr. S. Kaga of Heat Engine Laboratory of Nagoya University for his assistance in these experiments and to many fellow students of Nagoya University for their cooperation through their graduation theses.

References

1) J. P. Hartnett and E. R. G. Eckert: Trans. of A.S.M.E., Vol. 79 (1957), 751.
2) C. D. Pengelley: Jour. App. Phys., Vol. 28 (1957), 86.
3) R. G. Deissler and M. Perlmutter: Heat transfer and fluid mechanics institute, Preprints of paper, June 1958.
4) T. Ôno and O. Taniguchi: Trans. of Soc. of Mech. Engrs. (Japan), Vol. 17 (1951), 89.
5) H. C. Hottel and A. Kalitinsky: Jour. App. Mech., Vol. 12 (1945), 25.
6) A. H. Shapiro: The dynamics and thermodynamics of compressible fluid flow, I (1953), 83 (The Ronald Press Co.).